Solid State Ionics 308 (2017) 46–53

Contents lists available at ScienceDirect

Solid State Ionics

journal homepage: www.elsevier.com/locate/ssi

Formation of cubic Li_2TiO_3 by mechanical activation and its transformation to monoclinic phase: Stability in helium and hydrogen flows

I.A. Carbajal-Ramos[a,b,c,*], J.J. Andrade-Gamboa[a,c], A.M. Condó[a,b,c], F.C. Gennari[a,b,c]

[a] Instituto Balseiro (Universidad Nacional de Cuyo), Argentina
[b] Consejo Nacional de Investigaciones Científicas y Técnicas (CONICET), Argentina
[c] Centro Atómico Bariloche (Comisión Nacional de Energía Atómica), Argentina

ARTICLE INFO

Keywords:
Lithium titanium oxides
Mechanochemical synthesis
Physicochemical stability
Nuclear fusion
Batteries

ABSTRACT

Lithium metatitanate (Li_2TiO_3) is one of the most attractive candidates as a solid breeder in the blanket of D–T fusion reactors and ionic conductors in lithium-ion batteries. In this work, a new synthesis route, avoiding the use of solvents, high temperatures and dangerous sub-products, is used to obtain cubic and monoclinic Li_2TiO_3 nanopowders. This method consists of ball milling of LiCl, TiO_2 and NaOH in air atmosphere at room temperature and posterior calcination. Structural, microstructural and textural characteristics of the Li_2TiO_3 powders as well as of the pellets before and after annealing were determined. Remarkable contraction of the material and high mechanical stability was observed after treatment at 800 °C for 5 h. Finally, the behaviour in reductive and inert atmospheres of the sintered and green pellets was studied, characterizing the extension and impact of the reactions on the physicochemical and structural stability of the material. It can be concluded that the sintered pellets became mechanically stable due to the thermal treatment, showing no physicochemical modifications after analysis in different atmospheres up to 800 °C.

1. Introduction

Lithium metatitanate (Li_2TiO_3) is a lithium-based ceramic with a wide range of industrial applications. Among them, it is one of the most attractive candidates as a solid breeder in the blanket of the D–T fusion reactors [1–3] due to its properties (potentially high tritium generation, excellent tritium release at low temperature, reasonable lithium atom density, good compatibility with other materials at high temperatures, low chemical reactivity and high thermal stability). Also, Li_2TiO_3 is a promising component in microwave devices for the wireless and mobile communication industry, due to its good microwave dielectric properties (high quality factor, appropriate permittivity and near zero temperature coefficient of resonator frequency) [4]. Between other applications, Li_2TiO_3 is used as electrode material in lithium-ion batteries because its capacity of stabilize the high capacity cathode conducting agents and allow the occurrence of lithium diffusion [5].

Li_2TiO_3 possesses three structural modifications: α, β and γ [6,7]. The cubic α-Li_2TiO_3 (space group $Fm\bar{3}m$) is metastable and transforms irreversibly to the monoclinic β-Li_2TiO_3 (space group $C2/c$) above 300 °C [7]. The β-Li_2TiO_3 remains stable up to 1155 °C [6]. Above this temperature, it transforms reversibly to the cubic γ-Li_2TiO_3 (space group $Fm\bar{3}m$). The β-Li_2TiO_3 phase has a stoichiometric range from 47 to 51.5 mol% TiO_2 including at low temperature (from 600 to 1100 °C). Considering that the stoichiometry of the material has a strong influence in different properties such as thermal conductivity, thermal expansion, dielectric constant and ion mobility, it is an important factor to be modulated for industrial applications.

In previous investigations, β-Li_2TiO_3 has been usually synthesized by solid-state reaction using titanium dioxide (TiO_2) and lithium carbonate (Li_2CO_3) as starting materials [8–11] at temperatures above 800 °C. Although this method has the advantage of avoiding using solvents, it requires high temperatures and produces a material with poor diffusivity properties and large grain size. On the other hand, β-Li_2TiO_3 could also be obtained through some soft-chemical methods, such as sol–gel synthesis [12], hydrothermal [13,14], in-situ hydrolysis method [15], and solution combustion synthesis [16–18]. However, some of these synthesis procedures do not only generate large amounts of waste, but are also energy-intensive and expensive. In the case of α-Li_2TiO_3, it has been synthesized by a hydrothermal method with TiO_2 and LiOH as precursors and water as solvent [14]. However, this phase was not observed using others synthesis procedures [8–12].In this context, mechanochemical processing emerges as an alternative route to produce nanocrystalline solid materials, avoiding the use of solvents, expensive precursors and waste generation [19,20]. In this process

* Corresponding author.
E-mail address: alejandra.cbj@gmail.com (I.A. Carbajal-Ramos).

http://dx.doi.org/10.1016/j.ssi.2017.05.017
Received 26 March 2017; Received in revised form 19 May 2017; Accepted 26 May 2017

(during either ball milling or the subsequent low temperature heat treatment), precursors undergo a reaction to produce the required material which allows recovering an ultrafine powder. Although some previous studies produce Li_2TiO_3 or $Li_4Ti_5O_{12}$ by milling, Li_2CO_3 [21,22] and/or LiOH were used as precursors [23,24]. To the authors knowledge there are not any previous investigations on the synthesis of nanostructured Li_2TiO_3 by mechanochemistry processing of the LiCl and TiO_2 precursors with NaOH.

Structural, microstructural and textural characteristics of Li_2TiO_3 (like specific surface area, phase composition and crystallite size) are determined by the different synthesis routes and precursors used, which influence the properties and stability of the final material in operating conditions for different applications. In the case of breeder material in a fusion reactor this is worth considering since tritium release is favoured by low crystallite size and by adding H_2 into inert sweep gas [25,26]. In addition, in reducing atmospheres, titanium in Li_2TiO_3 can be reduced and lithium vaporisation can be increased [3,27], producing mass decrease and change in Li_2TiO_3 properties. Consequently, investigating the influence of the synthesis route on the microstructure and its relation with reduction behaviour of the synthesized Li_2TiO_3 becomes of great importance.

In the present work a new synthesis route to produce Li_2TiO_3 by mechanochemical reaction of LiCl and TiO_2 precursors with NaOH is developed. In order to evaluate the potentiality of the synthesized Li_2TiO_3 powders as breeder material, pellets of Li_2TiO_3 were heated under different atmospheres (helium, air and hydrogen) to analyse their physicochemical stability and their changes on the structure, microstructure and texture.

2. Experimental procedures

The starting materials used were anhydrous LiCl (Aldrich, 99%), TiO_2 (Aldrich, purity 99 wt%, anatase ≈ 75 wt% and rutile ≈ 25 wt%) and NaOH (Biopack, purity 98 wt%). The milling was carried out in a planetary ball mill (Fritsch Pulverisette P6), using both vial and balls of stainless steel. A ball to powder weight ratio of 53:1 was employed. Mixtures of 2.2 LiCl-1.0 TiO_2-2.2 NaOH powders were ball milled in air using 400 rpm for different periods of time. After milling, the samples were calcined in alumina crucible at 600 °C for 5 h and washed with water in order to eliminate NaCl produced as a sub-product of the reaction. The sample was dried at 120 °C overnight and it was calcined again at 600 °C for 24 h. The yield of the synthesis procedure was determined by calculation of the ratio between the experimental mass of Li_2TiO_3 obtained and the theoretical mass of Li_2TiO_3 expected according reaction (1).

Synthesized powders of Li_2TiO_3 were pressed by uniaxial compression (800 MPa) to produce green pellets (no binders added). Thermal treatment (800 °C for 5 h) was conducted on the green pellets in order to make them denser.

Structural and microstructural changes were studied by X-ray Powder Diffraction (XRPD), using PANaytical Empyrean equipment with graphite monochromator, CuKα radiation at 40 kV and 30 mA. X-ray diffractograms were collected using a step size of 0.013° and scan speed (°/s) of 0.0248. Textural characteristics of the samples were studied using a Micromeritics ASAP 2020 analyser. N_2 adsorption isotherms were collected at − 196 °C on 0.2 g of sample, after evacuation at 350 °C overnight. Surface area and pore distribution were obtained applying the BET and BJH methods, respectively. Solid phase IR spectra were obtained with an FTIR Perkin Elmer Spectrum 400 spectrometer in the range of 500–4000 cm^{-1}. The selected samples were grounded with dry KBr, pressed to pellets and put in a specially designed cell closed in an argon-filled glove box with moisture and oxygen content lower than 10 ppm. Morphological analyses of the samples were performed by Scanning Electron Microscopy (SEM Nova Nano 230, FEI Company) equipped with Energy Dispersive X-ray Spectroscopy (EDS) microanalysis. Transmission Electron Microscopy (TEM) studies were performed using either a Philips CM200 or a FEI Tecnai F20 G2 microscope operating at 200 kV. Samples for TEM were prepared by dispersing a small amount of powder in hexane and depositing a drop of the resulting suspension on a commercial holey-carbon coated copper grid. TEM cross sectional lamella was prepared with a Focused Ion Beam (FIB)/SEM dual beam system (FEI Helios Nanolab 650).

The thermal behaviour of the samples was studied under helium and hydrogen atmosphere by thermogravimetry (TG, TA Instruments HP50) using a heating rate of 10 °C min^{-1} and gas flow rate of 50 ml min^{-1}. The sample (about 80 mg) was maintained at room temperature for 30 min, in order to stabilize the baseline and remove physisorbed species. Then, it was heated to 800 °C, kept for 30 min and returned to its initial temperature. This cycle was repeated in order to obtain the baseline.

3. Results and discussion

3.1. Synthesis and characterization of cubic and monoclinic Li_2TiO_3 powders

The mechanochemical synthesis of Li_2TiO_3 powders from Li and Ti precursors in the presence of NaOH is a novel method, which is analogue to the synthesis procedure for oxide solid solutions developed by our group [28]. The expected reaction is thermodynamically favourable and can be expressed at room temperature as:

$$2LiCl(s) + TiO_2(s) + 2\,NaOH(s) \rightarrow Li_2TiO_3(s) + 2\,NaCl(s) + H_2O(l) \quad (1)$$

ΔG° (293 K) = − 168.3 kJ/mol [29]

In order to get the best milling conditions to produce reaction 1, preliminary tests were performed. In stoichiometric mixtures (2 LiCl-1 TiO_2-2 NaOH), the formation of monoclinic Li_2TiO_3 and cubic $Li_{4/3}Ti_{5/3}O_4$ was observed after combination of calcination, washing and calcination (see supplementary Fig. 1 of Appendix A). This indicates lithium loss and, as previous works have highlighted that an excess of lithium benefits the stability of the material [30], ball milling was implemented upon mixtures with 10 at.% Li excess (2.2 LiCl-1.0 TiO_2-2.2 NaOH).

Fig. 1 shows X-ray diffractograms for mixtures milled during different periods of time (15 min, 1 h, 2 h, 3 h and 5 h) and the assignations of reflections to the identified phases. In mixtures milled for 2 h to 5 h (Fig. 1c–e), the progressive advance of reaction 1 is observed, yielding Li_2TiO_3 as the metastable cubic phase. For shorter milling times (15 min, 1 h), NaCl is formed close to an intermediate phase, i.e. $LiOH{\cdot}H_2O$. This indicates that LiCl first reacts with NaOH to produce LiOH and NaCl, being this reaction thermodynamically favoured (reaction 2) [29]. However, no appreciable quantity of TiO_2 reacts with LiOH during this step (reaction 3). For 5 h of milling, the formation of α-Li_2TiO_3 is practically complete; while a minor amount of TiO_2

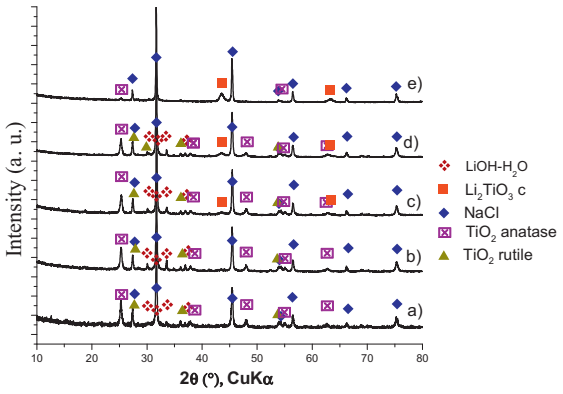

Fig. 1. XRPD patterns obtained after different milling times: a) 15 min, d) 1 h, c) 2 h, d) 3 h, and e) 5 h.

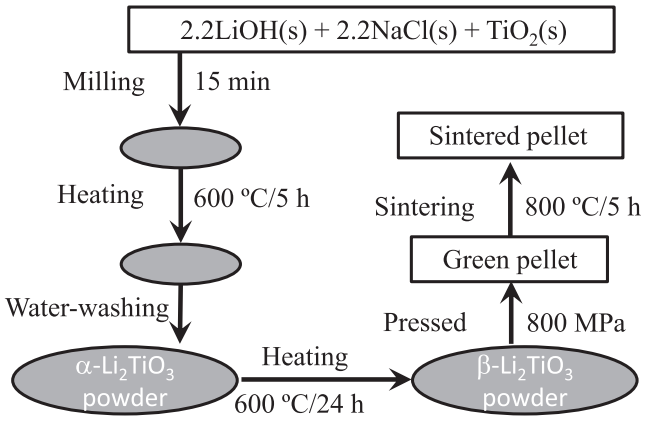

Scheme 1. Li_2TiO_3 powder and pellet synthesis procedure.

(anatase) remains. For all milling times, no $Ti(OH)_4$ was detected. These observations suggest that reaction 1 proceeds through a two-step process as follows:

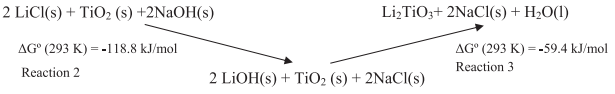

being both steps thermodynamically feasible [29].

To obtain Li_2TiO_3 as a unique final phase, the NaCl formed as co-product needs to be eliminated. The following sequence of treatments was applied after the milling: 1) calcinations in air at 600 °C for 5 h, 2) washings with water (to remove the NaCl), and 3) calcinations at 600 °C for 24 h (Scheme 1). As LiOH and LiCl are water-soluble compounds, the washing step should only be performed after complete reaction between LiOH and TiO_2. Fig. 2A and B show the XRPD analysis after that treatment upon samples milled for 15 min and 5 h, respectively. For both samples, reaction 1 is complete after the first calcination (Figs. 2Ab and Bb), obtaining the metastable cubic α-Li_2TiO_3structure. Also, incipient monoclinic β-Li_2TiO_3 is detected for both samples. The posterior water-washing step (Figs. 2Ac and Bc) fully removes the formed NaCl and the final calcination step (Figs. 2 Ad and Bd) allows the formation of the monoclinic β-Li_2TiO_3. Then, both processes lead to the successfully synthesis of Li_2TiO_3, with high yields of about 95%. The main difference among the previous procedures is that the formation of cubic Li_2TiO_3 requires a thermal treatment after 15 min of milling, whereas it occurs spontaneously after milling for 5 h (Fig. 1e). Then, long milling favours the occurrence of reaction 1 in the milling step (see Fig. 2Ba). However, the complete sequence of treatments leads to the same final product β-Li_2TiO_3 regardless of the milling time. It is worth mentioning that as the short duration of the first calcination prevents the reaction of Na^+ with TiO_2. In the follows, the synthesis procedure that involves the shortest milling time (15 min) was selected (Fig. 2Ad).

The cubic and monoclinic Li_2TiO_3 phases synthesized by the multi-step procedure were structural and microstructurally characterized. Calculations of crystallite size from X-ray difractograms were performed using the single peak method [31] and assuming spherical crystallites [32]: Lorentzian component of peak integral breadth allows to calculate mean crystallite size from Scherrer equation. For both cubic and monoclinic Li_2TiO_3, most intense peak was selected for calculation. The mean crystallite size of the cubic α-Li_2TiO_3 (Fig. 2Ac) was estimated as 13 nm [32]. It is worth highlighting that the cubic phase was stable during thermal treatment at 600 °C for 5 h, whereas Gicquel [7] and Laumann [33] had observed the cubic-monoclinic transformation at 300 °C. The extended stability range of cubic phase could be due to a crystallite size effect. As proposed for ZrO_2, an excess of surface energy of crystallites smaller than 30 nm may be the cause the existence of metastable tetragonal phase [34]. Crystallite size of cubic Li_2TiO_3 reported by Laumann [33] is 68 nm, i.e. almost one order of magnitude greater than our cubic phase. Additional research should be devoted to investigate in detail the causes of such stabilization. For monoclinic β-Li_2TiO_3 (Fig. 2Ad), the diffractogram in the 2θ range from 20° to 22° shows asymmetric line shapes typical for stacking faults [24]. The mean crystallite size (90 nm) could be calculated from the most intense reflection (2θ = 18.4°).

Fig. 3 shows the SEM micrograph of monoclinic Li_2TiO_3 compacted powder. The prevailing morphology of the powders consists of an agglomeration of rounded grains with mean sizes of 105 nm (measured over 100 grains). EDS analysis were performed and no impurities were observed on the limit of the technique. This average grain size and the mean crystallite size obtained by XRPD are almost the same. Then, each grain -as viewed by SEM- is practically a crystallite. Therefore, the milling process allows the formation of final phases in tiny domains of cubic Li_2TiO_3 (13 nm), which transform and grow as single crystals of monoclinic Li_2TiO_3 after the thermal treatment at 600 °C for 24 h.

The microstructure and structural homogeneity of the samples were further investigated employing TEM. Fig. 4 shows representative TEM results of monoclinic Li_2TiO_3 in bright field (BF), dark field (DF) and selected area electron diffraction (SAED) modes (Figs. 4a, b, c, respectively). Individual single crystals can be identified from the dark field image. The size distribution of the crystallites obtained from TEM is shown in the histogram in Fig. 4d with its corresponding log-normal fit. The mean crystallite size is 94 nm. This result is in good agreement

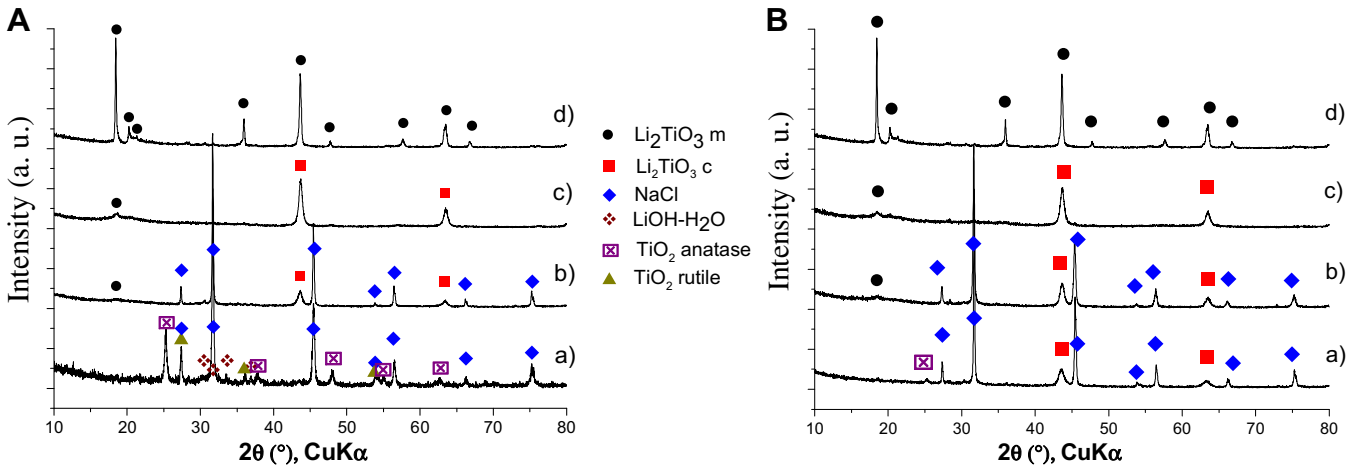

Fig. 2. XRPD patterns obtained for powder milled: **A)** during 15 min: a) as milled, b) after calcination at 600 °C for 5 h, c) after washed and d) after further calcination for 24 h at 600 °C. **B)** during 5 h: a) as milled, b) after calcination at 600 °C for 5 h, c) after washed and d) after further calcination for 24 h at 600 °C.

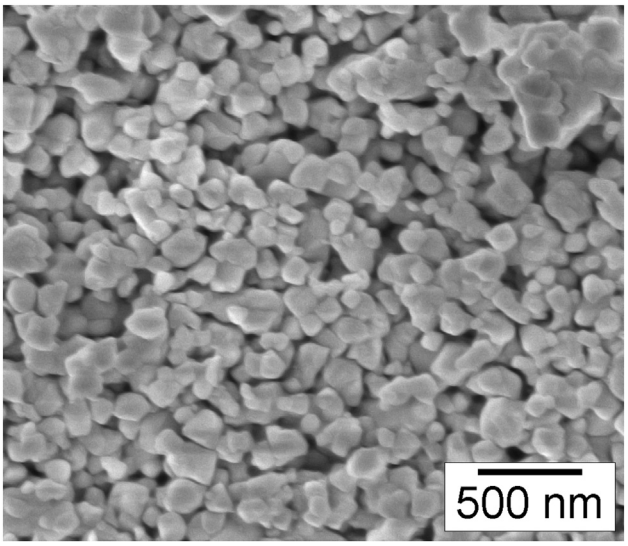

Fig. 3. SEM micrograph of monoclinic Li_2TiO_3 showing grain size distribution.

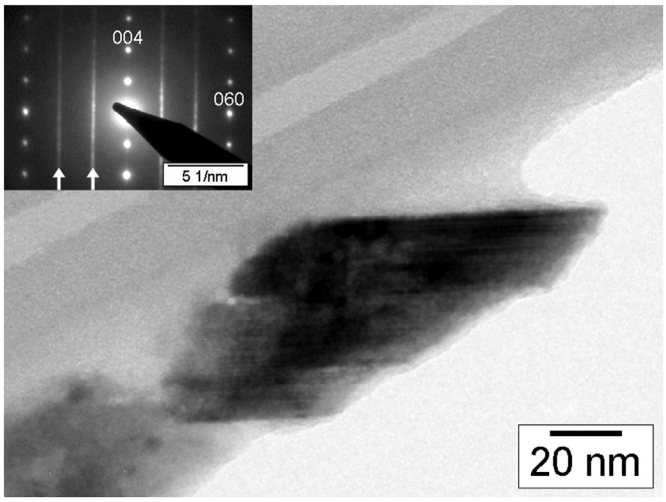

Fig. 5. Bright field image of a monoclinic Li_2TiO_3 grain with its corresponding electron diffraction pattern, which was indexed as [100] zone axis (inset).

with calculations from XRPD. The only presence of the monoclinic structure was confirmed on different SAED patterns. The simulated ring pattern for electron diffraction which corresponds to this structure [35] has been included in the pattern shown in Fig. 4c. It can be observed that most of the intense reflections of the SAED pattern match the rings. The reflections outside the rings can be indexed from the X-ray diffractogram included in the figure, corresponding to faint reflections of the same phase.

The presence of staking faults in several crystallites (suggested by XRPD) was confirmed by TEM. In the DF images they appear as parallel bright lines (indicated with arrows in Fig. 4b). In Fig. 5, one isolated grain is shown in a bright field image with its corresponding electron diffraction zone axis pattern (inset). Lines of diffuse scattering in the SAED pattern indicate stacking disorder [36]. Even though the zone axis was indexed as [100], the [110] zone axis could match as well, due to the spreading of reflections. The presence of stacking faults in β-Li_2TiO_3 formed by calcination at low temperature (< 700 °C) was also previously observed. It was reported that the stabilization of this imperfect state increases the mobility of the Li + ions in the structure [37]. This result is relevant because these defects could provide alternative channels for the diffusion of tritium inside the grain.

N_2 physisorption at the liquid nitrogen temperature was employed to investigate the evolution of the textural properties of the samples (see supplementary Fig. 2 of Appendix A). The surface areas of monoclinic and cubic Li_2TiO_3 were 11 $m^2\,g^{-1}$ and 100 $m^2\,g^{-1}$, respectively. Both samples present Type II isotherm, which displays the presence of macropores and some mesopores with undefined size and shape [38,39]. The hysteresis loops are slightly different, indicating disparity in the pore distribution. By applying the BJH method to the desorption branch of the isotherm, monoclinic Li_2TiO_3 possesses macropores > 50 nm, whereas the cubic phase shows a bimodal distribution: a small and wide pore size distribution (maximum at 3.5 nm) and a wide zone

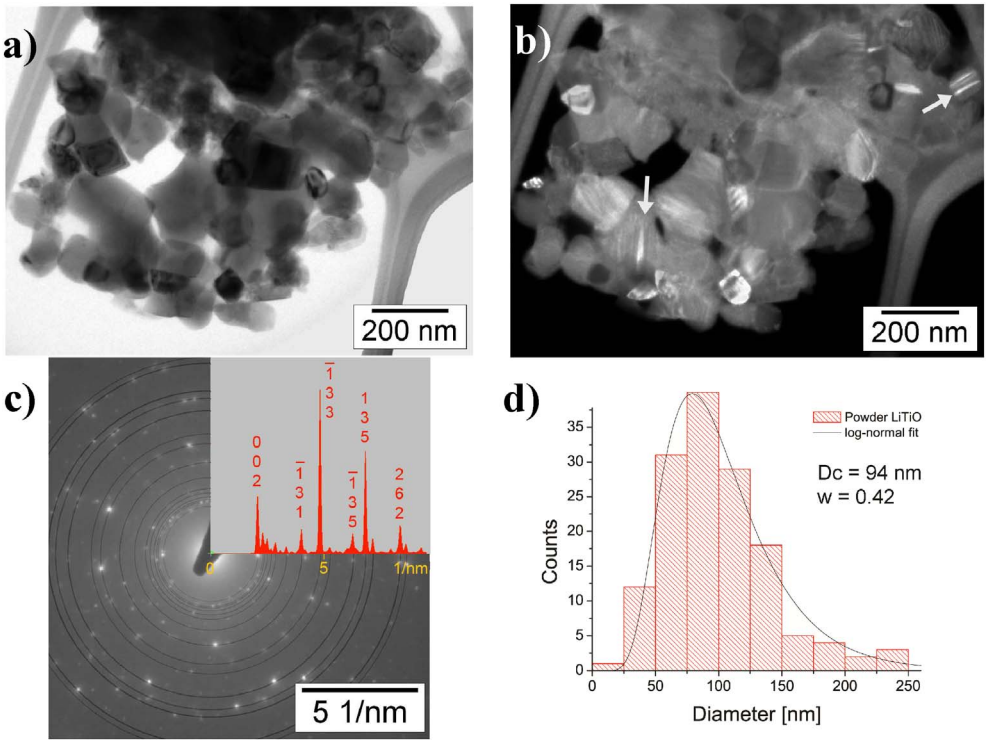

Fig. 4. TEM results corresponding to monoclinic Li_2TiO_3. a) Bright field image. b) Corresponding dark field image obtained with 002 reflection. c) SAED pattern indexed with the major reflections of the β monoclinic structure. d) Size distribution of crystallites and corresponding fit with log-normal distribution.

of macropores > 50 nm.

It can be concluded that metastable cubic Li_2TiO_3 (Fig. 2A, curve c) transforms into the stable monoclinic Li_2TiO_3 (Fig. 2A, curve d) after additional thermal heating at 600 °C for 24 h. This transformation involves reduction in one order of magnitude in the specific area and contraction in the pore volume comprising mesopores elimination. Accordingly, XRPD and TEM confirm a growth in grain size.

3.2. Preparation and characterization of monoclinic Li_2TiO_3 pellets

Several green pellets were obtained by uniaxial compression of the monoclinic Li_2TiO_3 powders previously produced (section 3.1) and were later calcined under mild conditions: 800 °C for 5 h (Scheme 1). The diameter and width of green pellets were approximately 6 mm and 1.5 mm, respectively. Their morphology remained the same as the powder. After sintering, shrinkage (final diameter 5 mm) and a remarkable increase in the hardness of the pellets were detected. The calculated densification was about 29% compared to the green pellet (calculated with the geometric density, $\delta_i = 1.95\ g\ cm^{-3}$, $\delta_f = 2.51\ g\ cm^{-3}$). The density of the pellet was 73% of the theoretical one, which is a reasonable value for the experimental conditions selected [40]. In addition, the sintered pellets maintained their structural integrity and did not evidence any cracks or breaks.

Fig. 6 shows and compares the XRPD patterns of the sintered pellet and Li_2TiO_3 powder. Both patterns look similar, and all peaks can be indexed based on monoclinic Li_2TiO_3 structure. The calculated crystallite size for sintered β-Li_2TiO_3 was 100 nm, slightly superior to the starting material. Sintered pellets also exhibit the presence of stacking faults (see Fig. 2Ad and related text), even when β-$Li_2TiO_3$was annealed at 800 °C. This observation is in agreement with a previous study of Laumann et al. [33]. These authors reported that during the cubic-monoclinic transformation, the β-Li_2TiO_3 obtained is disordered due to stacking faults and the complete transformation to the well-ordered monoclinic modification occurs above 1000 °C [41].

The textural study of the pellet (see supplementary Fig. 2 of Appendix A) shows an isotherm Type II without hysteresis, which denotes the presence of macropores with not well defined size and shape [38,39]. The surface area was $2\ m^2\ g^{-1}$.

SEM images of β-Li_2TiO_3 sintered pellet (external surface and cross section) are shown in Fig. 7. It can be seen that the Li_2TiO_3 pellets have faceted grains, with high grain boundary density and interconnected porosity. As mentioned before, Li_2TiO_3 powder has small crystallite size (around 90 nm) which coincides with the grain size. However, coarsening is observed in β-Li_2TiO_3 pellets and grain sizes reach values between 0.4 μm and 1.2 μm, as consequence of the compression and sintering treatment.

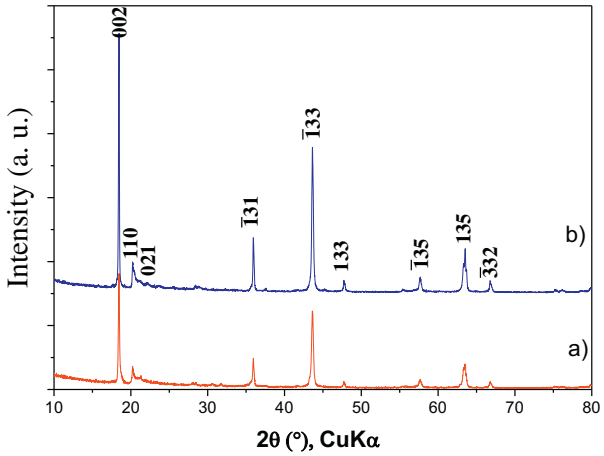

Fig. 6. XRPD patterns of a) monoclinic Li_2TiO_3 powders and b) sintered pellet with the major reflections indexed.

The microstructure of the sintered pellets was further investigated employing FIB and TEM (Fig. 8). A general overview of the grains and interconnected pores forming the pellets can be observed in the FIB lamella employing Scanning Transmission Electron Microscopy (STEM) in the dual beam system (Fig. 8a). By means of TEM, the different crystallites can be identified by SAED. The grain with stacking defects (circled in Fig. 8a) was oriented by TEM close to a zone axis (Fig. 8b) and identified as a crystallite of the monoclinic structure with stacking defects parallel to the (002) planes. The SAED pattern in Fig. 8b (inset) is similar to the one observed in Fig. 5, with lines of diffuse scattering along the same direction. The parallel lines observed inside some grains in the STEM image indicate the presence of stacking faults (arrows in Fig. 8a). The mean crystallite size in the pellets obtained by TEM is 500 nm with a distribution width of 400 nm. It is important to highlight that this is just an approximation, owing to the low number of crystallite used for this calculation. Considering that the crystallite size calculated by XRPD was 100 nm, the discrepancy with TEM observations could be ascribed to the presence of staking faults in the crystallites. Such type of defects broadens the XRPD peaks giving an inaccurate smaller crystallite size.

3.3. Thermal behaviour of monoclinic Li_2TiO_3 pellets in hydrogen and inert atmospheres

In order to evaluate the thermal stability of the monoclinic Li_2TiO_3 in different atmospheres, non-isothermal thermogravimetric analyses were performed. Fig. 9A shows the results corresponding to monoclinic Li_2TiO_3 phase using sintered and green pellets, both under He and H_2/Ar flow.

The Li_2TiO_3 green pellets in both atmospheres display two mass loss regimes, the first when heated up to 250 °C and the second between 250 and 450 °C. The first regime involves a mass loss of 0.55%, in He and 0.65% in H_2/Ar. The second one shows a mass loss of 0.89% in He and 1.17% in H_2/Ar. In addition, in H_2/Ar atmosphere a third regime with a 0.1% of mass loss is registered up to 800 °C. For Li_2TiO_3 sintered pellets, the total mass changes are significantly lower (0.13% and 0.26% in helium and H_2/Ar atmospheres, respectively). In fact, in H_2/Ar atmosphere, two zones of mass loss can be observed: the first one up to 350 °C (0.15% mass loss), and the second zone between 550 °C and 800 °C (0.11% mass loss).

In order to interpret the observed mass changes, FTIR analyses were carried out (Fig. 9B). Two samples were taken corresponding to the end of the two regimes of mass loss, indicated with arrows in TG curve. Before the TG experiments, a wide band is observed in Li_2TiO_3 green pellets at 3220 cm^{-1}, which can be attributed to OH vibration [42]. The two bands at 1441 cm^{-1} and 1497 cm^{-1} can be ascribed to carbonates associated with Li^+ ions, formed after capture of CO_2 from air [9,43]. Neither the band of hydroxyl was observed in the sample heated up to 300 °C (1), nor the hydroxyl or carbonate bands in the sample heated up to 500 °C (2). Therefore, it can be interpreted that first and second mass loss regimes are mainly associated with water and carbonates elimination, respectively. It can be concluded that after heating up to 500 °C, the samples surfaces are cleaned of all possible adsorbed and chemisorbed species. Similar FTIR spectra were observed for Li_2TiO_3 green pellets heated in helium atmosphere at the same temperature. Then, analogous processes (de-hydroxylation and carbonates releasing) are operating independently of the atmosphere for green pellets (Fig. 9A, curves c and d). On the other hand, the final mass loss observed in green pellets in H_2/Ar atmosphere between 500 °C and 800 °C (Fig. 9Ab) could be ascribed to reduction of Ti^{4+} to Ti^{3+}.

FTIR spectrum performed before the TG analysis shows that the bands corresponding to carbonates and hydroxyl disappeared (Fig. 9B) in sintered pellets. Considering that the sintered sample has low specific area, lesser carbonates and hydroxyls to desorb with heating are expected, in agreement with the lower mass loss exhibited by Li_2TiO_3 pellets (Fig. 9A, curves a and b). In fact, the thermal treatment at 800 °C

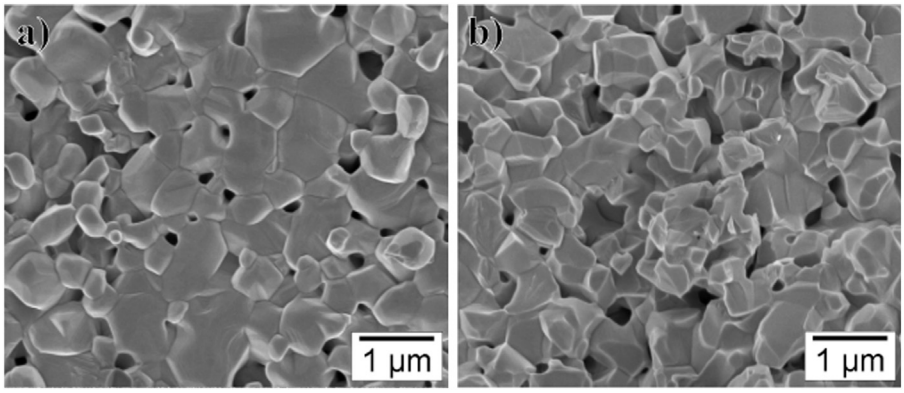

Fig. 7. SEM micrograph of a) the top and b) the cross section of Li_2TiO_3 sintered pellet.

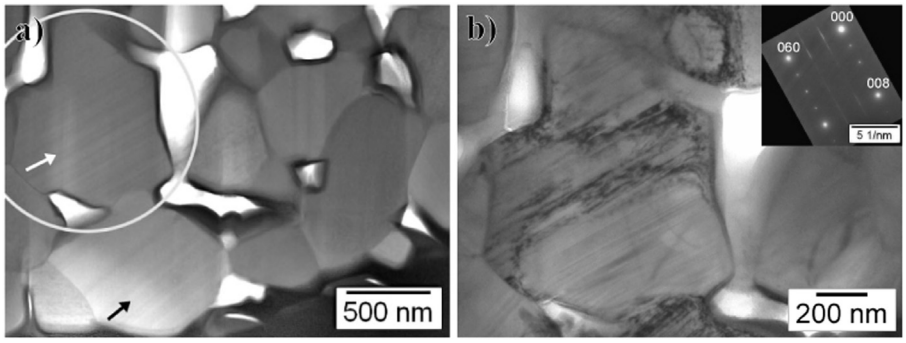

Fig. 8. Microstructure of the Li_2TiO_3sintered pellets. a) Bright field STEM image. The arrows indicate stacking defects. b) Bright field TEM image of the area selected by a circle in (a), near the zone axis shown in the SAED pattern (inset).

for 5 h favours the cleaning of the surface.

Treatments in H_2/Ar atmosphere (Figs.10a and 10b) cause a colour change from original white to deep grey. This colour change is also observed in the bulk of material, as it can be seen from pellets that were broken (Fig. 10a and b) to verify that hydrogen interaction is not only occurring at external surface. This effect, almost unobservable in helium atmosphere (Figs. 10c and d), indicates the presence of structural defects. In the present case, it can be associated with oxygen vacancies due to titanium reduction and according to the following reaction:

$$Li_2TiO_3(s) + xH_2(g) = Li_2TiO_{3-x}(s) + xH_2O(g) \quad (3)$$

Similar colour modification was observed by Hoshino et al. [3] in Li_2TiO_3 material upon heating under reducing atmosphere, suggesting

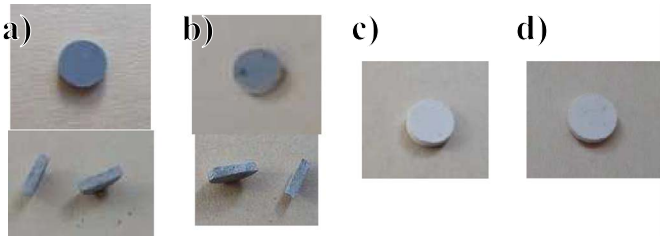

Fig. 10. Final colour of the sintered and green pellets of monoclinic Li_2TiO_3 after TG tests.

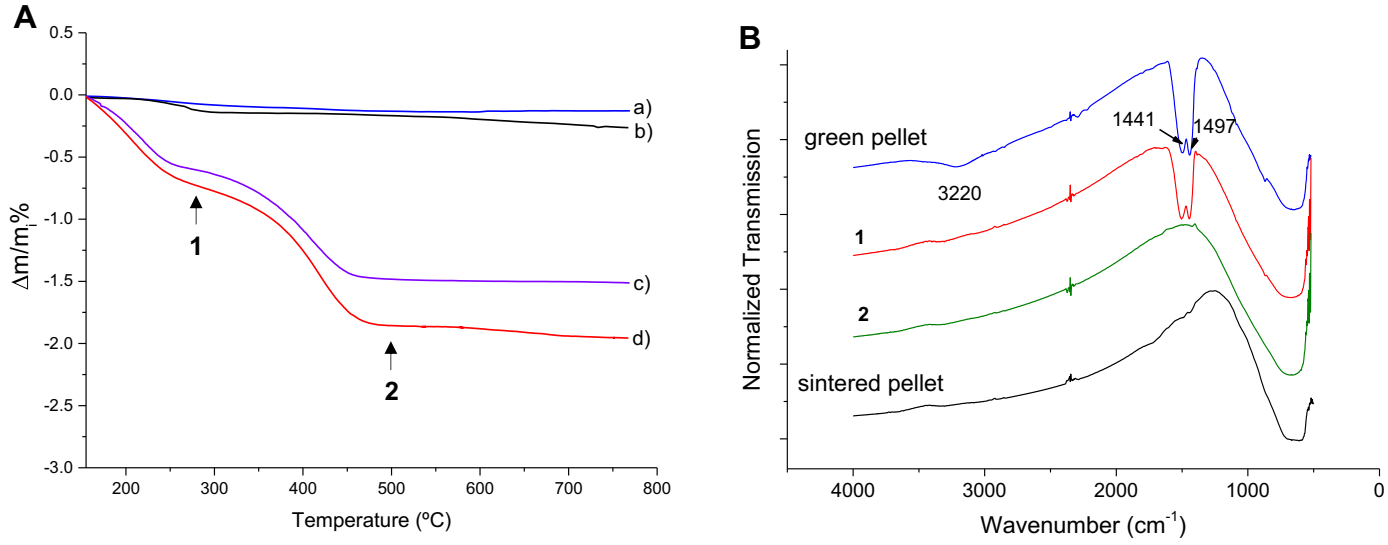

Fig. 9. A) Thermogravimetric analysis of monoclinic Li_2TiO_3. Sintered pellets: under a) He flow and b) H_2/Ar flow. Green pellets: under c) He flow and d) H_2/Ar flow. **B)** FTIR spectrum of the samples taken in arrows indicated as 1 and 2 compared with the initial green pellet and the sintered pellet. (For interpretation of the references to colour in this figure legend, the reader is referred to the web version of this article.)

that an oxygen vacancy is created and the charge compensated by Ti^{4+} reduction to Ti^{3+}.

Based on TG results, the reduction of titanium gives an x value < 0.01. For this extension of reduction, changes in lattice parameters are not expected [44]. The reduction degree observed is in agreement with other works about monoclinic Li_2TiO_3 reactivity with hydrogen [30,44]. Considering that in this study the H_2 concentration is 50 times superior than that used in the purge gas (100 Pa H_2) in a fusion reactor, the reduction of Li_2TiO_3 could be assumed negligible up to 800 °C.

XRPD patterns of Li_2TiO_3 sintered pellets before and after the treatment in different atmospheres are shown in supplementary Fig. 3 (see Appendix A). The sintered pellet after treatment in He flow does not exhibit new phases or detectable modifications. A similar observation was obtained for the material after treatment in H_2/Ar flow. In addition, FTIR analyses and SEM observations do not evidence detectable surface modifications. Considering that the sintered pellets were handled in air after TG curves, the stability toward hydroxylation and surface carbonation is demonstrated. This behaviour is desirable because the breeder will be loaded on the blanket in air atmosphere. Therefore, it is concluded that sintered pellets are mechanically stable and no new phases appear after thermal treatment under H_2/Ar or He atmospheres up to 800 °C. In addition, sintered pellets possess an interconnected network of pores and high boundary grain density that could improve the tritium release [26]. Additional studies will be performed for longer time and varying the temperature to investigate possible changes in the composition and/or stoichiometry of Li_2TiO_3.

4. Summary and conclusions

Cubic Li_2TiO_3 was successfully synthesized by mechanochemical processing of the 2.2 LiCl-1.0 TiO_2–2.2 NaOH mixture at room temperature. The starting mixture was milled, calcined, washed and calcined again. The final powder presented monoclinic phase, crystallite size of 100 nm and specific surface area of 11 m^2/g. In order to optimize the production process, different variables were considered: milling time, calcination time, washing/calcination sequence and composition of the starting mixture. A minimum milling time (15 min) could be achieved, with an initial composition of 10% excess of the LiCl and NaOH. The yield obtained was of 95% for the Li_2TiO_3 production. This monoclinic β-Li_2TiO_3 was produced through a new and versatile route, avoiding the use of solvents and at lower temperatures than the usual synthesis route (solid-state). In addition, under selected experimental conditions, cubic Li_2TiO_3 can be produced and it remains metastable in an extended temperature range (up to 600 °C) compared to bibliographic data.

Nanopowders of β-Li_2TiO_3were pressed into pellets by uniaxial compression without ligands. The green pellet shows a big mass loss due to elimination of surface hydroxyls and carbonates, and a final small mass loss due to Ti^{4+} to Ti^{3+} reduction in H_2/Ar atmosphere. Sintered pellet results thermally and mechanically stable in helium and H_2 atmosphere, showing a small reduction until 800 °C. Therefore, the high thermal stability, low chemical reactivity and the presence of stacking faults make these synthesized material as a promissory candidate as breeder blanket component.

Acknowledgements

This study has been partially supported by CONICET, CNEA, ANPCyT (PICT No. 1049) and Instituto Balseiro-University of Cuyo. The authors would like to thank Pablo Granell and Federico Golmar for the FIB lamella and the STEM image.

Appendix A. Supplementary data

Supplementary data to this article can be found online at http://dx.doi.org/10.1016/j.ssi.2017.05.017.

References

[1] J. G. van der Laan, A. V. Federov, S. van Til, J. Reimman, Ceramic breeder materials, in R Konings (Ed.), Comprehensive Nuclear Materials, 1st. Ed., Elsevier Science, 2012, pp. 463–510.
[2] M. Zmitko, et al., Development and qualification of functional materials for the EU Test Blanket Modules: strategy and R & D activities, J. Nucl. Mater. 417 (2011) 678–683, http://dx.doi.org/10.1016/j.jnucmat.2011.02.009.
[3] T. Hoshino, H. Kawamura, M. Dokiya, Y. Takahashi, T. Terai, M. Yamawaki, Non-stoichiometry of Li_2TiO_3 under hydrogen atmosphere conditions, J. Nucl. Mater. 329 (2004) 1300–1304, http://dx.doi.org/10.1016/j.jnucmat.2004.04.226.
[4] A. Sayyadi-Shahraki, E. Taheri-Nassaj, S.A. Hassanzadeh-Tabrizi, H. Barzegar-Bafrooei, A new temperature stable microwave dielectric ceramic with low-sintering temperature in Li_2TiO_3–$Li_2Zn_3Ti_4O_{12}$ system, J. Alloys Compd. 597 (2014) 161–166, http://dx.doi.org/10.1016/j.jallcom.2014.02.002.
[5] Z. Zhang, G. Hu, Y. Cao, J. Duan, K.D.Z. Peng, Enhanced electrochemical performance of nano $LiMnPO_4$ with multifunctional surface co-coating of Li_2TiO_3 and carbon, Solid State Ionics 283 (2015) 115–122, http://dx.doi.org/10.1016/j.ssi.2015.10.007.
[6] H. Kleykamp, Phase equilibria in the Li/Ti/O system and physical properties of Li_2TiO_3, Fusion Eng. Des. 61–62 (2002) 361–366, http://dx.doi.org/10.1016/S0920-3796(02)00120-5.
[7] C. Gicquel, M.M. Michel Mayer, R. Bouaziz, Sur quelquescomposésoxygénés du titane et des alcalines (Li, Na); étude des binaires M_2O-TiO_2dans les zones riches enoxydealcalin, C.R. Acad. Sci. Paris C 275 (1972) 1427–1430.
[8] Q. Zhou, Y. Gao, K. Liu, L. Xue, Y. Yan, Fabrication of Li_2TiO_3 pebbles by a selective laser sintering process, Fusion Eng. Des. 100 (2015) 166–170, http://dx.doi.org/10.1016/j.fusengdes.2015.05.061.
[9] R. Ramaraghavulu, S. Buddhudu, G. Bhaskar Kumar, Analysis of structural and thermal properties of Li_2TiO_3 ceramic powders, Ceram. Int. 37 (2011) 1245–1249, http://dx.doi.org/10.1016/j.ceramint.2010.12.007.
[10] X. Wu, Z. Wen, X. Xu, J. Han, Synthesis and ionic conductivity of Mg-doped Li_2TIO_3, Solid State Ionics 179 (2008) 1779–1782, http://dx.doi.org/10.1016/j.ssi.2008.03.001.
[11] O. Renoult, J.P. Boilot, J.P. Korb, M. Boncoeur, Lithium sol-gel ceramics for tritium breeding applications, J. Nucl. Mater. 223 (1995) 126–134, http://dx.doi.org/10.1016/0022-3115(95)00018-6.
[12] T. Hoshino, F. Oikawa, Trial fabrication tests of advanced tritium breeder pebbles using sol–gel method, Fusion Eng. Design 86 (2011) 2172–2175, http://dx.doi.org/10.1016/j.fusengdes.2011.01.065.
[13] W. Zhang, Q. Zhou, L. Xue, Y. Yan, Fabrication of Li_2TiO_3 pebbles with small grain size via hydrothermal and improved dry-rolling methods, J. Nucl. Mater. 464 (2015) 389–393, http://dx.doi.org/10.1016/j.jnucmat.2015.01.044.
[14] A. Laumann, K.T. Fehr, M. Wachsmann, M. Holzapfel, B.B. Iversen, Metastable formation of low temperature cubic Li_2TiO_3 under hydrothermal conditions-its stability and structural properties, Solid State Ionics 181 (2010) 1525–1529, http://dx.doi.org/10.1016/j.ssi.2010.08.017.
[15] Y.J. Li, C. Xu, X. Wang, L. Li, L. Kong, Synthesis of Li_2TiO_3 ceramic breeder powders by in-situ hydrolysis and its characterization, Mater. Lett. 89 (2012) 25–27, http://dx.doi.org/10.1016/j.matlet.2012.08.082.
[16] A. Sinha, S.R. Nair, P.K. Sinha, Single step synthesis of Li_2TiO_3 powder, J. Nucl.Mater. 399 (2010) 162–166, http://dx.doi.org/10.1016/j.jnucmat.2010.01.013.
[17] C.H. Jung, J.Y. Park, S.J. Oh, H.K. Park, Y.S. Kim, D.K. Kim, J.H. Kim, Synthesis of Li_2TiO_3 ceramic breeder powders by the combustion process, J. Nucl. Mater. 253 (1998) 203–212, http://dx.doi.org/10.1016/S0022-3115(97)00313-9.
[18] M. Hong, Y. Zhang, M. Xiang, Y. Zhang, Reprocessing of lithium titanate pebbles by graphite bed method, J. Nucl. Mater. 455 (2014) 311–315, http://dx.doi.org/10.1016/j.jnucmat.2014.06.054.
[19] C. Suryanarayana, Mechanical alloying and milling, Prog. Mater. Sci. 46 (2001) 1–184, http://dx.doi.org/10.1016/S0079-6425(99)00010-9.
[20] V.V. Zyryanov, Mechanochemical synthesis of complex oxides, Russ. Chem. Rev. 77 (2008) 105–135, http://dx.doi.org/10.1070/RC2008v077n02ABEH003709.
[21] Z.-F. Fu, P. Liu, J.-L. Ma, Fabrication nanopowders by high-energy ball-milling and low temperature sintering Li_2TiO_3 microwave dielectrics, Mater. Sci. Eng. B 193 (2015) 32–36, http://dx.doi.org/10.1016/j.mseb.2014.11.004.
[22] R. Padhy, N. Rao, S.K.S. Parashar, K. Parashar, P. Chaudhuri, Sintering effect on electrical properties of Li_2TiO_3, Solid State Ionics 256 (2014) 29–37, http://dx.doi.org/10.1016/j.ssi.2013.12.031.
[23] I. Veljković, D. Poleti, Lj. Karanović, M. Zdujić, G. Branković, Solid state synthesis of extra phase-pure $Li_4Ti_5O_{12}$ spinel, Sci. Sinter. 43 (2011) 343–35, , http://dx.doi.org/10.2298/SOS1103343V.
[24] G. Wang, J. Xu, M. Wen, R. Cai, R. Ran, Z. Shao, Influence of high-energy ball milling of precursor on the morphology and electrochemical performance of $Li_4Ti_5O_{12}$ ball-milling time, Solid State Ionics 179 (2008) 946–950, http://dx.doi.org/10.1016/j.ssi.2008.03.032.
[25] K. Tsuchiya, M. Nakamichi, A. Kikukawa, Y. Nagao, M. Enoeda, T. Osaki, K. Ioki, H. Kawamura, In-pile test of Li_2TiO_3 pebble bed with neutron pulse operation, J. Nucl. Mater. 307–311 (2002) 817–822, http://dx.doi.org/10.1016/S0022-3115(02)01304-1.
[26] E. Carella, M. Gonzalez, R. Gonzalez-Arrabal, D-depth profiling in as-implanted and annealed Li-based breeder blanket ceramics, J. Nucl. Mater. 438 (2013) 193–198, http://dx.doi.org/10.1016/j.jnucmat.2013.02.073.
[27] T. Hoshino, M. Dokiya, T. Terai, Y. Takahashi, M. Yamawaki, Non-stoichiometry and its effect on thermal properties of Li_2TiO_3, Fusion Eng. Des. 61–62 (2002)

353–360, http://dx.doi.org/10.1016/S0920-3796(02)00216-8.
[28] I.A. Carbajal Ramos, J.J. Andrade Gamboa, F.C. Gennari, Nanostructured $Ce_{1-x}Zr_xO_2$ solid solutions produced by mechanochemical processing, Mater. Chem. Phys. 137 (2013) 1073–1080, http://dx.doi.org/10.1016/j.matchemphys.2012.11.039.
[29] H.S.C. Outokumpu, Chemistry For Windows, Version 6.1, Outokumpu Research Oy, Finland, 2009.
[30] T. Hoshino, K. Sasaki, K. Tsuchiya, K. Hayashi, A. Suzuki, T. Hashimoto, T. Terai, Crystal structure of advanced lithium titanate with lithium oxide additives, J. Nucl. Mater. 386–388 (2009) 1098–1101, http://dx.doi.org/10.1016/j.jnucmat.2008.12.289.
31 J.I. Langford, R.D.E. Delhez, ThH. Keijser, E.J. Mittemeijer, Profile analysis for microcrystalline properties by the Fourier and other methods, Aust. J. Phys. 41 (1988) 173–187, http://dx.doi.org/10.1071/PH880173.
[32] C.E. Kril, R. Birringer, Estimating grain-size distributions in nanocrystalline materials from X-ray diffraction profile analysis, Philosophical Magazine A 77 (3) (1998) 621–640, http://dx.doi.org/10.1080/01418619808224072.
[33] A. Laumann, K.T. Fehr, H. Boysen, M. Hölzel, M. Holzapfel, Temperature-dependent structural transformations of hydrothermally synthesized cubic Li_2TiO_3 studied by in-situ neutron diffraction, Z. Kristallogr. 226 (2011) 53–61, http://dx.doi.org/10.1524/zkri.2011.1286.
[34] R.C. Garvie. The occurrence of metastable tetragonal zirconia as a crystallite size effect, J. Phys. Chem. 69 (1965) 1238-1243. DOI: http://dx.doi.org/10.1021/j100888a024.
[35] C.L. Yu, F. Wang, S.-Y. Cao, D.-P. Gao, H.-B. Hui, Y.-Y. Guo, D.-Y. Wang, The structure of H_2TiO_3—a short discussion on “Lithium recovery from salt lake brine by H_2TiO_3”, Dalton Trans. 44 (2015) 15721–15724, http://dx.doi.org/10.1039/c4dt03689a.
[36] N.V. Tarakina, T.A. Denisova, Y.V. Baklanova, L.G. Maksimova, V.G. Zubkov, R.B. Neder, Defect crystal structure of low temperature modifications of Li_2MO_3 (M=Ti, Sn) and related hydroxides, Advances in Science and Technology 63 (2010) 352–357, http://dx.doi.org/10.4028/www.scientific.net/AST.63.352.
[37] N.V. Tarakina, R.B. Neder, T.A. Denisova, L.G. Maksimo, Y.V. Baklanova, A.P. Tyutyunnik, V.G. Zubkov, Defect crystal structure of new $TiO(OH)_2$ hydroxide and related lithium saltLi_2TiO_3, Dalton Trans. 39 (2010) 8168–8176, http://dx.doi.org/10.1039/c0dt00354a.
[38] M. Thommes, K. Kaneko, A.V. Neimark, J.P. Olivier, F. Rodriguez-Reinoso, J. Rouquerol, K.S.W. Sing, Physisorption of gases, with special reference to the evaluation of surface area and pore size distribution (IUPAC Technical Report), Pure Appl. Chem. 87 (9–10) (2015) 1051–1069, http://dx.doi.org/10.1515/pac-2014-1117.
[39] F. Rouquerol, J. Rouquerol, K.S.W. Sing, P. Llewellyn, G. Maurin, Adsorption by Powders and Porous Solids Principles, Methodology and Applications, 2nd. ed., Elsevier Science, 2014.
[40] Th. Fehr, E. Schmidbauer, Electrical conductivity of Li_2TiO_3 ceramics, Solid State Ionics 178 (2007) 35–41, http://dx.doi.org/10.1016/j.ssi.2006.11.002.
[41] A. Laumann, K.M.Ø. Jensen, C. Tyrsted, M. Bremholm, K.T. Fehr, M. Holzapfe, B.B. Iversen, In-situ synchrotron X-ray diffraction study of the formation of cubic li_2tio_3under hydrothermal conditions, Eur.J.Inorg.Chem. (2011) 2221–2226, http://dx.doi.org/10.1002/ejic.201001133.
[42] M.R. Mohammadi, D.J. Fray, Low temperature nanostructured lithium titanates: controlling the phase composition, crystal structure and surface area, J. Sol-Gel Sci. Technol. 55 (2010) 19–35, http://dx.doi.org/10.1007/s10971-010-2209-6.
[43] D.R. Zhang, H.L. Liu, R.H. Jin, N.Z. Zhang, Y.X. Liu, Y.S. Kang, Synthesis and characterization of nanocrystalline $LiTiO_2$ using a onestep hydrothermal method, J. Ind. Eng. Chem. 13 (2007) 92–96 (ISSN: 1226086X).
[44] C. Alvant, S. Casadio, V. Contint, R. Giorgi, M.R. Mancint, K. Tsuchiya, H. Kawamura, Li Depletion Effects on Li_2TiO_3 Reaction with H_2 in Thermo-chemical Environment Relevant to Breeding Blanket for Fusion Power Plants, JAERI Review, Vol. 024 (2005) (RT/2005/2/MAT(ENEA)).